

Laboratory 04 – Metallography and Steel Analysis

Nate Abrams, Jeffrey Harrick, and Jay Parmar

April 9, 2025

1 Introduction

The purpose of this lab is to identify three unknown metal samples (annealed steel, quenched steel, and cast iron) by using hardness testing and microscopy analysis. This process will require knowledge of crystal structure, material properties, processing techniques/effects, and data analysis. These concepts, taught in lecture, will be expanded upon with reinforced learning throughout this lab. First, the samples were fixed in a plastic composite, which was sanded and polished to produce a flat metallic surface. Hardness tests of the metals were taken during Lab 3, while Lab 4 required acidic etching of each samples before the crystal structure was viewed under a microscope.

2 Background

Understanding what microstructures make up steel is an essential component of determining its identity. Annealing and quenching are two different methods of steel manufacturing (heat treating) that create unique internal structures^[1]. A quenched sample is rapidly cooled from high temperatures, typically in water, which traps the high-temperature phases in a distorted, hard form called martensite. Annealing involves slowly cooling the sample in a furnace, which allows for softer (and oftentimes more stable) phases like ferrite and pearlite^[1]. Cast iron is known to have the highest carbon content of all three specimens studied in this report. While it may be heat treated, the high carbon content leads to the formation of graphite flakes or cementite. These features make cast iron brittle, but very strong. Each phase has its own characteristic. Ferrite, which forms at low carbon contents, is relatively soft and ductile. This phase (87%) combines with cementite (13%) to form pearlite, a layered microstructure that results from the slow cooling of annealed steel. The type and distribution of these phases directly influence the steel's hardness and mechanical behavior, as examined with the hardness test (higher carbon content is usually stronger)^[2]. Using the metallography techniques of this lab, the specimens can be identified, as each of the phases displays a unique pattern or structure. For example, pearlite can often be identified by the long, alternating, “finger-like” strands of carbon and iron (see Appendix 1).

This lab is especially relevant to the real world, as steel is known to be the most commonly found structural material in engineering. It is frequently used in automotive, aerospace, civil infrastructure, biomedical devices, and countless other fields. While it is important to understand the physical properties resulting from each of these manufacturing techniques, it is just as important to understand why these changes occur. For example, understanding why Young's modulus for a material is what it is allows engineers to make more educated assumptions when designing different products. Metallographic etching and imaging techniques, such as those used in this experiment, help reveal these underlying properties by exposing microstructures critical to performance^[4]. Through this experiment, the team gains hands-on experience with metallographic preparation techniques and learns how to apply theoretical knowledge to real engineering problems.

3 Experimental Procedure & Materials

The experiment began with sectioning, which was completed in advance by the lab manager. Stock material—ranging from 3/4 inch to 5/8 inch diameter rods and 1/2 inch rectangular bars—was cut into smaller specimens while preserving the original microstructure. The three unknown metal samples prepared for analysis were cast iron, annealed steel, and quenched steel. Initial hardness measurements for each were performed during Lab 3 using a Rockwell Hardness Testing Machine.

During Lab 3, the samples were mounted using a molding press with powdered Bakelite to form easy-to-handle pucks. Once mounted, each specimen underwent grinding using a rotary sanding machine equipped with water-assisted silicon carbide sandpaper. Coarse grinding removed surface deformation from sectioning, while fine grinding at higher grits prepared the surface for polishing.

The polished stage was completed using a rotary polishing wheel and an alumina-based polishing solution. This step removed the fine scratches left from grinding and produced a mirror-like finish required for microscopic evaluation.

Initial observations were made using an inverted optical microscope at 50x magnification, though minimal features were visible due to the un-etched state of the samples.

To reveal the microstructure, each specimen was etched using Nital — a solution of 1–4% nitric acid (HNO_3) in ethanol — applied with a cotton swab. Immediately after etching, the samples were rinsed with alcohol and dried using a hot air gun to avoid introducing contaminants or scratches.

Post-etching, the samples were re-examined at 500x magnification using the same inverted microscope. At this stage, grain boundaries and phase structures became visible. If the microstructure was unclear or over/under-etched, samples were re-polished and etched again before being re-evaluated. Digital images were captured using microscope imaging software for further analysis.

Microstructure analysis was carried out using two primary methods: the line/circle intercept method for grain size measurement and point counting to estimate phase fractions. By comparing the observed micro-structural features and hardness values, each sample was identified based on structural characteristics, relative hardness, and inferred carbon content.

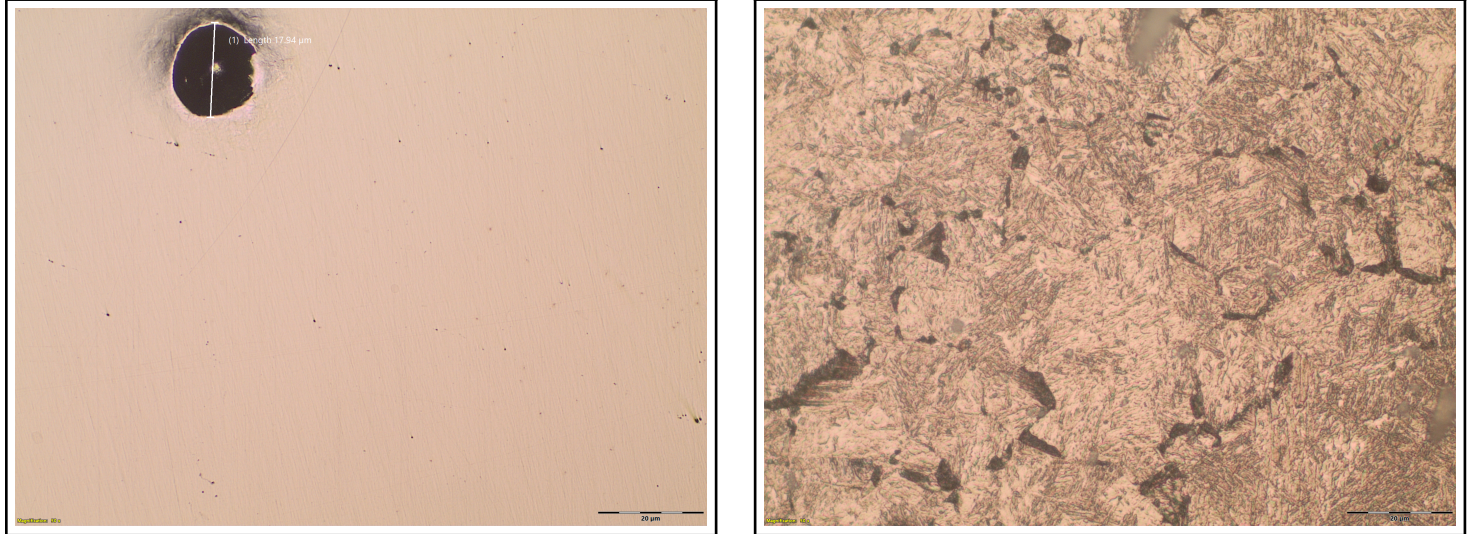
The data collected included digital photos of each specimen before and after etching, qualitative visual observations of micro-structural features, and quantitative hardness measurements using the Rockwell Hardness Testing Machine.

4 Results

Table 1: Raw experimental hardness data

| Sample | Inner Hardness | Inner Average | Outer Hardness | Outer Average |
|--------|------------------------------|---------------|------------------------------------|---------------|
| A | 81.5, 82.0, 82.0, 82.0, 82.5 | 82.0 | 81, 81, 80.5, 80.5, 80.5, 80.5 | 80.7 |
| B | 60.5, 60.5, 61.0, 61.5, 61.5 | 60.7 | 62.0, 63.0, 63.0, 62.5, 62.5, 62.0 | 62.5 |
| C | 61.0, 61.0, 60.5, 59.0, 60.5 | 60.4 | 57.0, 56.5, 55.5, 57.5, 56.5, 58.0 | 56.8 |

Table 1 presents the raw Rockwell hardness (scale A) measurements for the three specimens. Specimen A exhibits the highest overall hardness, with slightly higher values recorded on the outer surface. This gradient suggests a rapid cooling process, where the outer regions solidified first, trapping bonds in a higher-energy, harder state, while the interior cooled more slowly. Specimen B shows a more balanced hardness profile between the inner and outer regions, indicating a more uniform cooling rate. Specimen C demonstrates the lowest hardness overall, likely due to slower cooling that allowed for grain growth and the development of a softer microstructure.

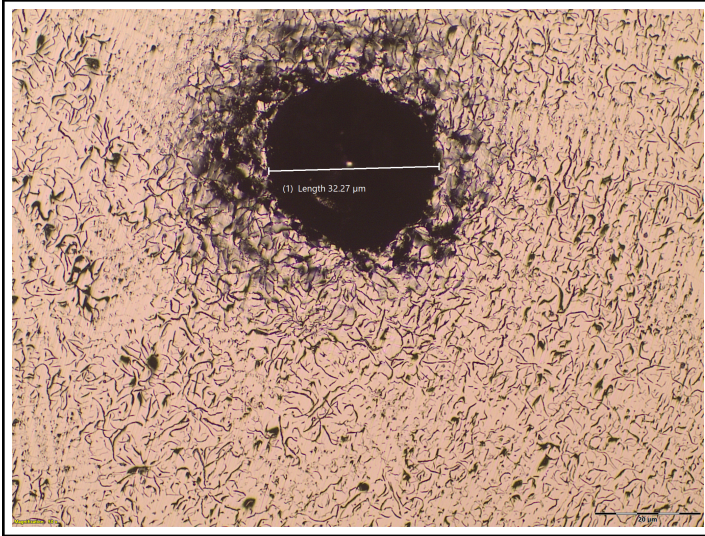


(a) Specimen A before etching at 50x magnification

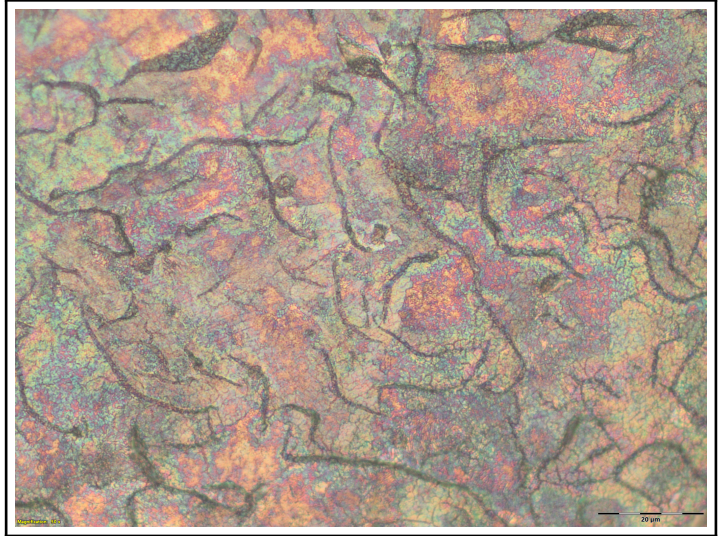
(b) Specimen A after etching at 500x magnification

Figure 1: Photos of Specimen A

Specimen A initially displays a uniform surface under 50x magnification, with minimal surface irregularities aside from the dents from hardness testing, Figure 1(a). Post-etching, the microstructure at 500x magnification reveals small, needle-like grains interspersed among larger, indistinct grain boundaries are characteristics of a rapid cooling process in steel, Figure 1(b). These needle-like features are characteristic of martensite, a hard, brittle phase formed during rapid cooling. The carbon distribution within the steel appears more uniform than in Specimen B (Figure 2), though still not as homogeneously dispersed as in Specimen C (Figure 3).



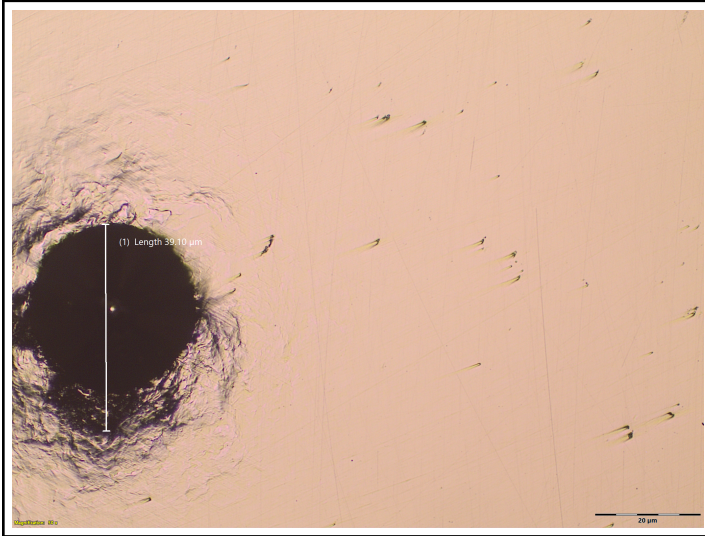
(a) Specimen B before etching at 50x magnification



(b) Specimen B after etching at 500x magnification

Figure 2: Photos of Specimen B

Specimen B exhibits a non-uniform surface at 50x magnification before etching, containing a multitude of small black veins of carbon deposits. The dent from hardness testing is also visible in Figure 2(a). After etching, the microstructure at 500x magnification emphasizes these carbon deposits. The image appears significantly darker than the other specimens, and upon closer inspection, reveals fine, thread-like carbon structures branching between the more prominent graphite veins. This characteristic of graphite flakes embedded within ferrite and possibly pearlite, key features of slow cooling. The visible carbon-iron layering and the high carbon content further support this identification, suggesting a slow cooling process that allowed free carbon to form the vein structures.



(a) Specimen C before etching at 50x magnification



(b) Specimen C after etching at 500x magnification

Figure 3: Photos of Specimen C

Specimen C presents a relatively uniform surface at 50x magnification, similar in appearance to Specimen A prior to etching, Figure 3 (a). However, the etched microstructure at 500x reveals significantly larger and somewhat more defined grain structures Figure 3 (b). The grain structures are still not particularly clear in many areas of the image, making it challenging to determine the grain size of the sample. The presence of these coarse grains and the absence of concentrated carbon regions suggest that the material underwent a much slower cooling process, allowing ample time for grain growth and diffusion. This is further supported by the significantly greater quantity of pearlite than ferrite, as seen in the 500x magnification, Figure 3 (b). The slow cooling not only allows for coarse grain growth and homogeneous carbon diffusion but also promotes a more complete eutectoid transformation, resulting in a microstructure dominated by pearlite. We observed little to no ferrite in this sample.

4.1 Area Fraction and Grain Size Calculations

We can find the grain size by finding a ratio of the total length of the circumference of the circle with the total number of intersections that the circle makes with the grain boundaries. As the grain boundaries are not always clearly defined, we took our best estimate in five randomly distributed circles of radius 10 μm :

$$\frac{2\pi \times 10 \times 5}{(4 + 4 + 4 + 4 + 4)} = 15.708 \mu\text{m}$$

10x3 square grids were arranged to estimate the area fraction, however, the entire image showed little to no evidence of visible ferrite.

Table 2: Quantitative analysis for sample C

| Parameter | Average Grain Size | Area Fraction | Standard Deviation |
|-----------|----------------------|----------------|--------------------|
| Sample C | 15.708 μm | ~100% pearlite | ~0% |

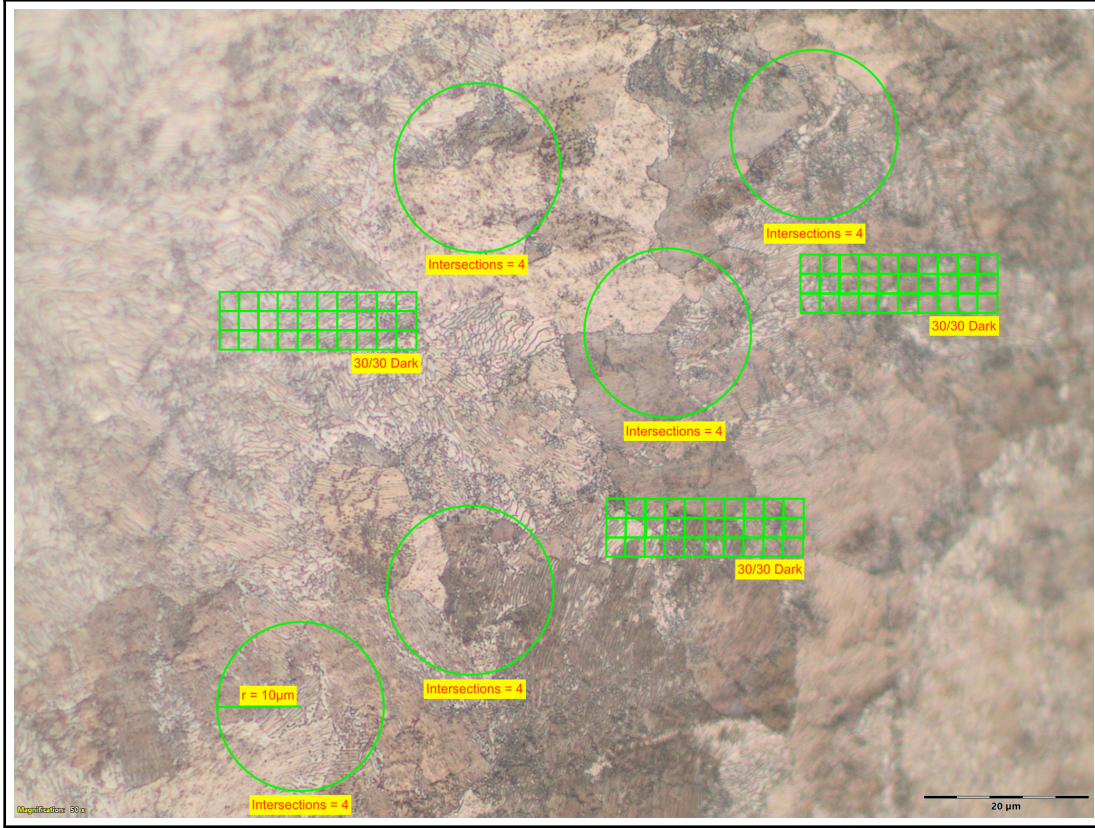


Figure 4: Specimen C Area Fraction and Grain Size Analysis

5 Discussion

5.1 Analysis of Results

5.1.1 Specimen A

As stated above, specimen A shows clear signs of the martensite phase in the sample. As shown in Figure 4 (Appendix) the alternating, finger-like pattern is seen can be closely tied to martensite. This phase is typically the result of the phases found when heated metal that is being processed is cooled extremely quickly. Martensite is a stable structure at these elevated temperatures, and when the specimen is rapidly cooled (in water), the phase does not have time to shift, allowing this phase to be seen at room temperature. Unlike pearlite (to some extent), it is difficult to distinguish individual grain boundaries in the post-etching images of specimen A. This seemingly random orientation can be attributed to the high internal stress that the steel encounters at the high temperatures. The chart identifies martensite as having a carbon content of .5%. Lastly, data from the previous lab session (Table 1) shows specimen A as having the highest hardness values. Once again this aligns

with the quenching process as rapid cooling traps carbon atoms in a distorted, strained lattice that resists deformation. Using all of this analysis, it is suggested that **Specimen A is quenched steel**. Most likely one of the following, **1045 carbon steel, 1018 carbon steel, A36 steel, and 8620 steel alloys**, which matches the shown carbon content of .5%.

5.1.2 Specimen B

As shown in Figure 2, Specimen B exhibits a notably high carbon content, clearly visible even prior to etching. The carbon inclusions are prominent and far more abundant than those observed in Specimens A and C. This elevated carbon concentration is characteristic of cast iron, particularly due to the presence of substantial graphite deposits. These deposits form during the smelting process, where carbon is introduced. During the slow cooling rate the carbon deposits partially diffuse through the iron matrix. This diffusion contributes to the formation of pearlite and the transformation of what would otherwise be ferrite regions—explaining the relative scarcity of ferrite observed in the microstructure. Further evidence supporting the identification of Specimen B as cast iron comes from its hardness: lower than that of Specimen A but slightly higher than an annealed sample. This intermediate hardness aligns with gray cast iron, which cools slowly enough to allow carbon redistribution without forming high-hardness martensite. Based on micro-structural features and mechanical properties, **Specimen B is most likely gray cast iron (ASTM A48)** with a carbon content exceeding 1.5%.

5.1.3 Specimen C

Based on the microstructural features and hardness data, the sample with relatively large, coarse grains, a nearly exclusive pearlite structure (with virtually no visible ferrite), and the lowest hardness of the three is most consistent with an annealed treatment. Annealing promotes slow cooling that facilitates significant grain growth through recrystallization and allows for the complete diffusion of carbon, leading to a predominantly pearlitic microstructure, a behavior often observed in steels near the eutectoid composition. Considering the list of metals, four likely candidates include 1010 carbon steel, 1018 carbon steel, 1045 carbon steel, and 1075 carbon steel. However, both 1010 and 1018 are low-carbon steels that typically contain a substantial amount of ferrite along with pearlite, and 1045 tends to develop a mixed microstructure with appreciable primary ferrite. In contrast, 1075 carbon steel, with its higher carbon content near the eutectoid level, is predisposed to form an almost entirely pearlitic structure when annealed, resulting in a softer material with coarse grains. Thus, the observed characteristics indicate that **Specimen C is most likely annealed 1075 carbon steel** with a known carbon content between 0.7% and 0.8%. Below, we compute the carbon content based on our estimate of the area fraction, and find it to be very consistent with the known carbon content of 1075 carbon steel.

$$\text{carbon content \%} = 0.0076 \times (100\%) = 0.76\% \text{ carbon}$$

5.2 Sources of Error

A potential source of error may have originated during the initial sizing of the samples. However, subsequent grinding and polishing would have removed most surface-level damage affecting the grain structure. Furthermore, improper grinding or polishing could leave residual surface deformation, which would decrease the clarity of the micro-structural features.

During etching, errors may arise from over-etching or under-etching the sample. Over-etching exaggerates grain boundaries and obscure finer details, while under-etching may fail to sufficiently reveal the microstructure, making interpretation inaccurate.

Another source of error is post-etch handling. Once polished and etched, samples are vulnerable to scratches, fingerprints, or debris, all of which can interfere with image clarity.

Lastly, human error plays its usual role in image analysis. Misreading microscope images can skew data and calculating carbon content using the grid and circle methods introduces uncertainty, especially when done by eye rather than with image analysis software.

6 Conclusion

This lab used hardness testing and microscopy analysis to determine the identity of 3 unknown steel specimens. Specimen A was determined to be quenched steel. The finger-like composition and heightened hardness of specimen A is consistent with the martensite phase. Moreover, the carbon content of .5% suggests it is most likely, 1045 carbon steel, 1018 carbon steel, A36 steel, and 8620 steel alloys. Specimen B was identified as cast iron due to the notably high carbon content shown in the large, dark black carbon veins shown on the post-etching image. This is consistent with ASTM A48 grey cast iron. Finally, specimen C was suggested to be annealed steel on account of its clearly defined pearlite, lack of ferrite, and large grain structure. These stable crystals are usually the result of slow, drawn out cooling times which allow for proper phase adjustment within the metal. This, in conjunction with the lower hardness testing data indicates that this metal was 1075 carbon steel, 1045 carbon steel, 1010 steel, and 1018 steel alloys. The similar lists of possibilities for both specimen A and C is concurrent with the lab manual that states both are the same steel just differing in how they were heat treated.

7 References

References

- [1] “Carbon Steels.” *Total Materia*, <https://www.totalmateria.com/page.aspx?ID=SteelArticles&LN=EN&NM=Carbon%20Steels>. Accessed 1 Apr. 2025.
- [2] “What Is Metallography?” *Metallography.com*, https://www.metallography.com/what_is_metallography.htm. Accessed 1 Apr. 2025.
- [3] “Sample Preparation Equipment.” *Buehler*, <https://www.buehler.com/sample-preparation.php>. Accessed 1 Apr. 2025.
- [4] “Metallographic Etching.” *Materials Evaluation and Engineering*, <https://www.mee-inc.com/hamm/etching/>. Accessed 1 Apr. 2025.
- [5] Suryanarayana, C. “Methods of Quantitative Metallography.” *ResearchGate*, https://www.researchgate.net/publication/301553438_Methods_of_Quantitative_Metallography. Accessed 1 Apr. 2025.

8 Appendix

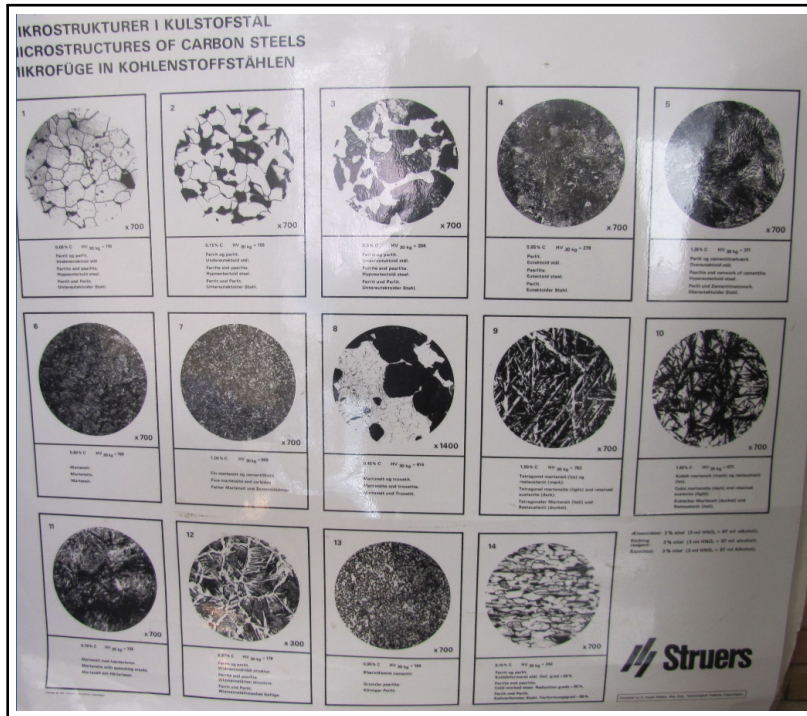


Figure 5: Images of microstructure of known steels

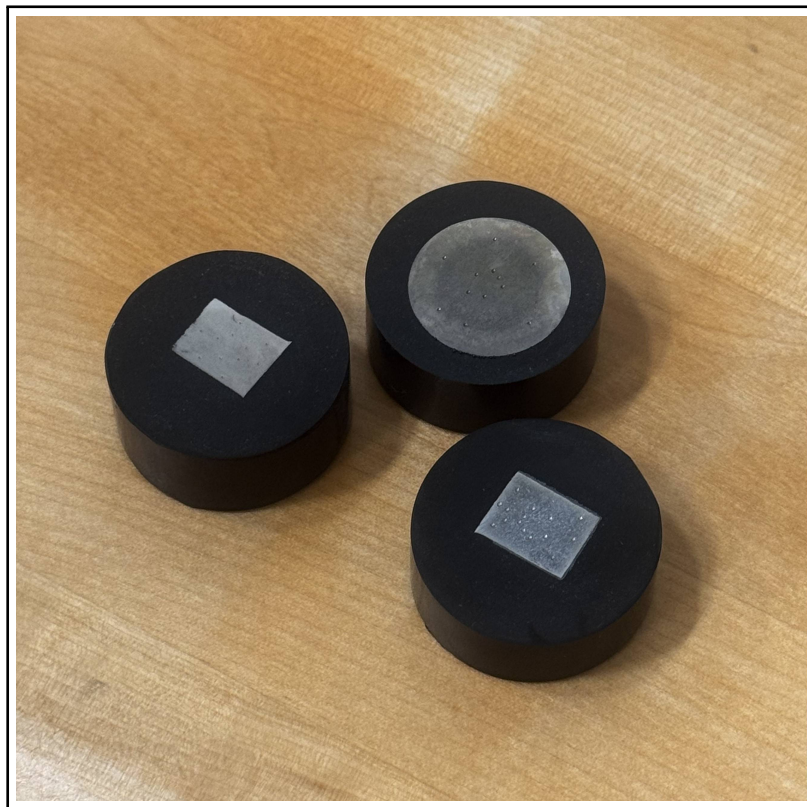


Figure 6: Experimental Specimens (from left to right A, B, C)